Intrinsic Structural Transitions of the Pyramidal I $\langle \mathbf{c} + \mathbf{a} \rangle$ Dislocation in Magnesium

Zhaoxuan Wu[a,b,*], W. A. Curtin[a]

[a] *Institute of Mechanical Engineering, École Polytechnique Fédérale de Lausanne, Lausanne CH-1015, Switzerland*
[b] *Institute of High Performance Computing, 1 Fusionopolis Way, #16-16, Connexis, Singapore 138632, Singapore*

Abstract

The stability of a mixed $\langle \mathbf{c}+\mathbf{a} \rangle$ dislocation on the pyramidal I plane in magnesium is studied using molecular dynamics simulations. The dislocation is metastable and undergoes a thermally-activated transition to either a sessile, basal-dissociated $\langle \mathbf{c} + \mathbf{a} \rangle$ or a sessile basal-dissociated $\langle \mathbf{c} \rangle$ dislocation plus an $\langle \mathbf{a} \rangle$ dislocation. The transition is intrinsic to magnesium and occurs with an energy barrier of $\sim$0.3 eV. Extensive easy-glide dislocation slip with $\langle \mathbf{c} + \mathbf{a} \rangle$ Burgers vector is thus not sustainable on either pyramidal I or II planes. Enhancing the ductility of magnesium by stabilizing $\langle \mathbf{c} + \mathbf{a} \rangle$ slip on the pyramidal I plane thus appears unlikely to be viable.

Keywords: Magnesium, Dislocations, Plasticity, Molecular Dynamics Simulations

In hexagonal close-packed (hcp) metals, dislocation slip with $\langle \mathbf{c} + \mathbf{a} \rangle$ Burgers vector is an important deformation mode to accommodate c-axis strain [1, 2]. In magnesium (Mg), recent molecular dynamics (MD) simulations [3] show that the key pyramidal II $\langle \mathbf{c} + \mathbf{a} \rangle$ dislocation is metastable on the easy-glide pyramidal II plane and undergoes an intrinsic transition into basal-dissociated dislocation structures. The transition is thermally activated, predicted to occur at very high rates at room temperature, and results in sessile dislocations that can not contribute to plastic strain and serve as strong barriers to all dislocation slip systems [4, 5]. The unusual climb-dissociated dislocation structure found in MD is consistent

*Corresponding author
Email address: zhaoxuan.wu@epfl.ch (Zhaoxuan Wu)

with past [6, 7] and very recent [8, 9] TEM observations where a high density of $\langle \mathbf{c}+\mathbf{a} \rangle$ edge dislocations lie preferentially along the intersection of the pyramidal II and basal planes ($\boldsymbol{\xi}_2$-$[\bar{1}010]$ direction in Fig. 1). This transition of the pyramidal II $\langle \mathbf{c}+\mathbf{a} \rangle$ dislocation was thus postulated to be the origin of the high strain hardening, low ductility, and early failure of Mg. To enhance the ductility of Mg, one strategy could be to energetically stabilize the $\langle \mathbf{c}+\mathbf{a} \rangle$ dislocation through solution additions so that the undesirable transition could be delayed to longer times or higher temperatures. A second strategy could be to alloy the material so as to stabilize the $\langle \mathbf{c}+\mathbf{a} \rangle$ dislocation on the pyramidal I plane, relative to the pyramidal II plane, with assumed easy glide on the pyramidal I plane. The first step in assessing the latter strategy is to establish the stability of $\langle \mathbf{c}+\mathbf{a} \rangle$ dislocations on the pyramidal I plane.

In this work, we present MD simulations that show that an initial $\langle \mathbf{c}+\mathbf{a} \rangle$ dislocation dissociated on the pyramidal I plane is metastable and undergoes transitions into lower-energy, basal-dissociated, sessile dislocation structures, similar to transitions reported recently for the pyramidal II $\langle \mathbf{c}+\mathbf{a} \rangle$ dislocation. The energy barrier for the transition is $\sim$0.3 eV, lower than the $\sim$0.5 eV for the dislocation transition on pyramidal II plane, and thus occurring even faster than in the pyramidal II case. These results suggest that $\langle \mathbf{c}+\mathbf{a} \rangle$ dislocation on pyramidal I plane can not provide sustained dislocation plasticity, so that a strategy of shifting the stability of the $\langle \mathbf{c}+\mathbf{a} \rangle$ dislocation onto that plane, or a strategy to activate $\langle \mathbf{c}+\mathbf{a} \rangle$ slip on both pyramidal I and II planes, is not likely to succeed in enhancing ductility.

The simulation model and methods follow closely our recent work [3]. We create a perfect hcp lattice having x in the pyramidal I plane, y normal to the pyramidal I plane, and z along the $\boldsymbol{\xi}_1$ direction (see Fig. 1). The $\langle \mathbf{c}+\mathbf{a} \rangle$ dislocation is constructed using the Volterra procedure where atoms are first displaced according to the anisotropic elastic displacement field [10] of a straight dislocation along the z direction with $\langle \mathbf{c}+\mathbf{a} \rangle$ Burgers vector, followed by relaxation with atoms within $2r_c$ ($2\times$ the cut off distance of the potential) held fixed at their elastic displacement solutions and periodic boundary conditions applied in the dislocation line direction (z). The resulting dislocation has a mixed character, consisting of a 60° basal $\langle \mathbf{a} \rangle$ dislocation and an edge $\langle \mathbf{c} \rangle$ dislocation. For the finite temperature simulations, atom positions are first scaled from the T = 0 K to those appropriate at the finite temperature lattice parameters, and atom velocities are then assigned randomly according to a Gaussian distribution around the desired mean velocity at the desired temperature. A Nosé-Hoover thermostat [11, 12, 13, 14] is used to maintain constant temperature. All simulations here are performed under zero applied stress. The MD simulations are performed using

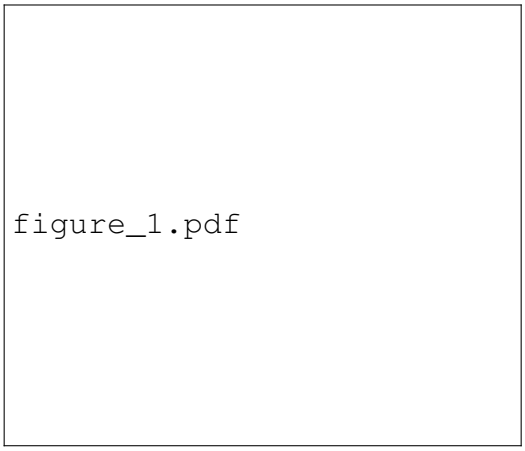

Figure 1: Schematic diagram of $\langle \mathbf{c}+\mathbf{a} \rangle$ dislocations on the pyramidal I and II planes, indicating the line directions for the mixed pyramidal I dislocation at the intersection of the basal and pyramidal I planes ($\boldsymbol{\xi}_1$-$[\bar{2}110]$) and the edge pyramidal II dislocation at the intersection of the basal and pyramidal II planes ($\boldsymbol{\xi}_2$-$[\bar{1}010]$).

the Large-scale Atomic/Molecular Massively Parallel Simulator (LAMMPS) [15]. The interatomic Mg interactions are described with a modified embedded-atom method (MEAM)-type interatomic potential specifically parametrized for simulating dislocation plasticity and fracture phenomena of Mg [16]. All energy minimizations are carried out using a conjugate gradient algorithm. Atomic structures are identified using common neighbor analysis [17].

To probe the stability of the initial dislocation on the pyramidal I glide plane, we perform MD simulations at various temperatures (400, 500, 600 and 700 K) and using different sizes and boundary conditions, similar to the earlier work [3]. The initial dislocation is metastable and undergoes transition into basal-dissociated structures. Figure 2 shows the transition at 500 K where the $\langle \mathbf{c}+\mathbf{a} \rangle$ dislocation dissociated on the pyramidal I plane transforms into $\langle \mathbf{c} \rangle$ and $\langle \mathbf{a} \rangle$ in close proximity (Fig. 2a) or into a basal-dissociated $\langle \mathbf{c}+\mathbf{a} \rangle$ dislocation (Fig. 2b). The transition process is similar, but not identical to that of $\langle \mathbf{c}+\mathbf{a} \rangle$ dislocation on pyramidal II plane [3]. For the pyramidal I case, a basal $\langle \mathbf{a} \rangle$ Shockley partial dislocation is first nucleated and glides a short distance, leaving behind an intrinsic I_2 basal stacking fault. The trailing Shockley partial $\langle \mathbf{a} \rangle$ is often nucleated subsequently, resulting in a 60° $\langle \mathbf{a} \rangle$ and a full edge $\langle \mathbf{c} \rangle$ dislocation in close proximity (see middle column of Fig. 2). The $\langle \mathbf{c} \rangle$ dislocation then climb-dissociates onto the basal plane, creating an extrinsic basal stacking fault and making the $\langle \mathbf{c} \rangle$ effectively

Figure 2: Transition of $\langle \mathbf{c}+\mathbf{a} \rangle$ dislocation on pyramidal I plane into basal-dissociated dislocations at 500 K. (a) and (b) show nominally identical MD simulations at the indicated times but leading to different final structures. The rightmost schematics show the transition of dislocation Burgers vectors before (solid purple arrow) and after (dashed blue arrows) the transition. In all atomic images, atoms are colored on the basis of common neighbour analysis: blue = hcp; green = fcc; purple = bcc; yellow = all others. Dislocation core atoms thus appear predominantly as yellow and the stacking fault atoms on the basal plane appear as green. Dislocation cores are indicated by the Burgers vector symbol "$\perp$".

sessile. Presumably, the $\langle \mathbf{a} \rangle$ dislocation will glide away under sufficiently high resolved stresses on basal plane, leaving behind the sessile $\langle \mathbf{c} \rangle$ dislocation. In the current stress-free simulations, the $\langle \mathbf{a} \rangle$ dislocation remains close to the $\langle \mathbf{c} \rangle$ due to short range interactions between the two cores. In some cases, the $\langle \mathbf{a} \rangle$ and $\langle \mathbf{c} \rangle$ dislocations combine and transform into a pair of basal-dissociated $\langle \mathbf{c} + \mathbf{a} \rangle$ partial dislocations having a basal I_1 stacking fault in between, as shown in Fig. 2b. Overall, the resulting dislocation structures are similar to those found in the transition of pyramidal II $\langle \mathbf{c} + \mathbf{a} \rangle$ dislocations, but the dislocation line direction is along $\boldsymbol{\xi}_1$-$[\bar{2}110]$.

To measure the transition rates and estimate the associated energy barrier, we perform a massive set of MD simulations using simulation cell has dimensions ($l_x \times l_y \times l_z$) of ∼30 nm × 30 nm × 3.2 nm with boundary atoms fixed at their elastic displacement solution. Transition times are measured on at least twenty nominally identical simulations at each temperature. Figure 3a shows the mean transition time $\bar{t}$ versus temperature T, as measured in the MD simulations. For comparison, the mean transition time for the pyramidal II dislocation measured previously is also shown. At the same temperature, $\bar{t}$ for the pyramidal I dislocation is at least an order of magnitude smaller than that for the pyramidal II dislocation, indicating that the easy-glide $\langle \mathbf{c} + \mathbf{a} \rangle$ dislocation is less stable on the pyramidal I plane than on pyramidal II plane. The mean transition rate $R = 1/\bar{t}$ can be related to the transition energy barrier ΔE using the Arrhenius law $R = \nu_0 \exp^{-\Delta E/(kT)}$, where ν_0 and k are the attempt frequency and Boltzmann constant, respectively. Fig 3b shows the estimated ΔE versus T for both pyramidal I and II dislocations, using ν_0 = 10^{13}s^{-1}. Overall, the transition has an energy barrier of ∼0.3 eV, which is rather lower than the ∼0.5 eV for pyramidal II dislocations.

A large simulation cell with long dislocation line length (∼30 nm × 30 nm × 32 nm) with fixed boundary conditions (open circles in Fig. 3) and a large simulation cell with large in-plane dimensions (∼250 nm × 250 nm × 3.2 nm) with free surface boundary conditions (half-filled circle in Fig. 3) in the x and y directions are used to examine the effects of simulation cell size and boundary conditions on the observed transition. However, neither simulation cell size nor the fixed boundary have any significant effects on the transition rate, energy barrier, or type of transitions.

The thermally activated transitions are driven by a reduction in the dislocation energy. All the new dislocation structures have lower energy than the initial dislocation dissociated on the pyramidal I plane, again similar to the pyramidal II case. In all pyramidal I cases, the dislocation core and its associated defects (see Fig. 2)

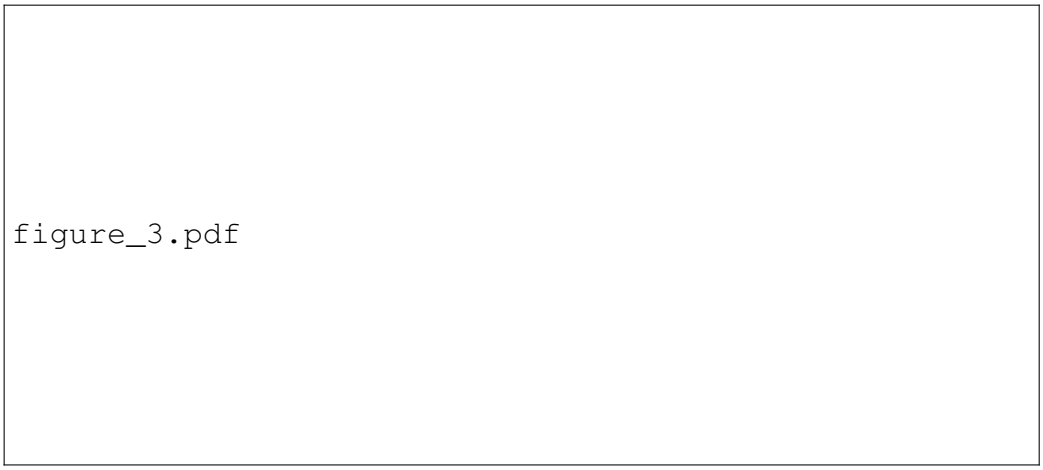

Figure 3: Thermally activated mean transition time and energy barrier for the pyramidal I to basal plane transformation. (a) Mean transition time $\bar{t}$ versus temperature T as measured in MD for the dissociation events shown in Fig. 2. (b) Energy barrier ΔE for the thermally activated transitions, showing a small dependence on temperature. Error bars (s.e.m., n = 2) indicate the 95% confidence intervals of the mean transition time and energy barrier. Open and half-filled circles indicate (nearly identical) results obtained for larger simulation cells and different boundary conditions. The results for pyramidal II dislocation are also shown for comparison.

are contained within some distance r_{min} around the core region. We can therefore express the total dislocation energy E_{tot} per unit length within a cylindrical region of radius r centered at the dislocation core as $E_{tot} = E_{struc} + E_{elastic}$, where E_{struc} is the energy within r_{min} and depends on the details of the atomic structure around the core region while $E_{elastic}$ is the additional elastic energy between r_{min} and r and is independent of atomic structure around the core region. $E_{elastic}$ scales as $K \ln(r/r_{min})$ [10], where K is a constant completely determined by the anisotropic elastic constants, total Burgers vector $\boldsymbol{b}$ contained within r_{min}, and dislocation line direction $\boldsymbol{\xi}$. Since the Burgers vector and crystal orientation are the same for all structures studied here, the constant K is the same for all dislocation structures, independent of the dislocation dissociation, stacking faults, etc. In contrast, the quantity E_{struc} depends on the details of the dislocation structure in each case. Thus, the *differences* in total energy $E_{tot}(r)$ at large $r > r_{min}$ reflect differences in the "core" energies, stacking faults, and elastic interactions among all of the dislocations and defects inside r_{min}. This difference is the quantity of physical importance since it provides the thermodynamic driving force for the transitions. This difference is also perfectly well-defined and measurable atomistically without approximation.

Figure 4 shows the atomistically-calculated total dislocation energy per unit length E_{tot} versus $\ln(r/r_{min})$. The $\langle \mathbf{c}+\mathbf{a} \rangle$ dislocation dissociated on the pyramidal I plane has the highest energy, followed by the $\langle \mathbf{c} \rangle$ plus $\langle \mathbf{a} \rangle$ in close proximity, and with the $\langle \mathbf{c}+\mathbf{a} \rangle$ climb-dissociated on basal plane having the lowest energy. Both the total reduction of dislocation energy of $\sim$0.3 eV/Å and the order of the dislocation energy with different structures are similar to results for the pyramidal II $\langle \mathbf{c}+\mathbf{a} \rangle$ dislocation. Specifically, in both pyramidal I and II planes, the basal-oriented, climb-dissociated $\langle \mathbf{c}+\mathbf{a} \rangle$ dislocations have the lowest energy and are the most stable core configurations. Unfortunately, these low-energy climb-dissociated $\langle \mathbf{c}+\mathbf{a} \rangle$ and $\langle \mathbf{c} \rangle$ core structures are sessile and cannot contribute to plastic slip.

Our simulations have some implications for the relative importance of pyramidal I and pyramidal II slip in Mg. The simulations indicate that $\langle \mathbf{c}+\mathbf{a} \rangle$ slip on pyramidal I plane will result in sessile, basal-dissociated $\langle \mathbf{c}+\mathbf{a} \rangle$ and $\langle \mathbf{c} \rangle$ dislocations lying along the $\boldsymbol{\xi}_1$-$[\bar{2}110]$ direction. If $\langle \mathbf{c}+\mathbf{a} \rangle$ pyramidal I slip were significant, one would expect a high density of such sessile dislocations left behind after c-axis plastic deformation. All TEM studies to date report sessile dislocations primarily aligned with the $\boldsymbol{\xi}_2$-$[\bar{1}010]$ direction, indicating that they formed from pyramidal II dislocations. Observations of sessile dislocations with $\boldsymbol{\xi}_1$-$[\bar{2}110]$ line direction are not common. While further TEM quantification of such disloca-

Figure 4: Dislocation energy vs dislocation structure. (a) Total dislocation energy within a cylindrical region of radius $r > r_{min} = 6b$ for the $\langle \mathbf{c} + \mathbf{a} \rangle$ mixed dislocation on the pyramidal I plane (purple circles; case i), for edge $\langle \mathbf{c} \rangle$ and 60° $\langle \mathbf{a} \rangle$ in close proximity (orange squares; case ii), and for $\langle \mathbf{c} + \mathbf{a} \rangle$ mixed dislocation climb-dissociated on the basal plane (open blue squares; case iii). Here, b is the magnitude of the $\langle \mathbf{c} + \mathbf{a} \rangle$ dislocation Burgers vector. The analytical energy prefactor K (the slope) from the anisotropic elastic solution is also shown (solid lines). (b) Dislocation core structures corresponding to the energies shown in (a) (case i, ii and iii) as computed at zero temperature.

tions may provide more insight into the relative slip activity on both pyramidal planes, the existing literature suggests that pyramidal II is dominant. In forthcoming work, we will present analysis of the pyramidal I and II *screw* dislocations, and the process of cross-slip between them. Nudged elastic band [18, 19] (NEB) calculations therein will show that the energy barrier for $\langle \mathbf{c}+\mathbf{a} \rangle$ cross-slip between the pyramidal II and the pyramidal I planes is on the order of $\sim$0.5 eV. With such a relatively low cross-slip energy barrier, easy cross-slip of the $\langle \mathbf{c}+\mathbf{a} \rangle$ screw dislocation can be expected so that some plastic slip on the pyramidal I plane is feasible even if pyramidal II slip is dominant, particularly under c-axis tensile loading and at high temperatures. Recent experiments using slip trace analysis [20, 21] do suggest that $\langle \mathbf{c}+\mathbf{a} \rangle$ slip can occur on the pyramidal I plane. These findings could raise the hope of increasing the c-axis plastic strain capacity of Mg by activating or stabilizing pyramidal I $\langle \mathbf{c}+\mathbf{a} \rangle$ slip. Our results of a transition to various basal-dissociated sessile dislocation structures, expected to occur rapidly at room temperature, indicate that even if $\langle \mathbf{c}+\mathbf{a} \rangle$ slip could be activated on the pyramidal I plane, *sustainable* c-axis plastic deformation in Mg seems unlikely. We would expect the material would still exhibit high work hardening and low ductility, particularly in c-axis deformation. Therefore, the conceptual strategy of stabilizing the $\langle \mathbf{c}+\mathbf{a} \rangle$ on the pyramidal I plane to achieve high ductility appears unlikely to be successful.

In light of the results for both pyramidal II and pyramidal I $\langle \mathbf{c}+\mathbf{a} \rangle$ structures, the design of ductile magnesium remains daunting. We believe that one possible strategy is to introduce solutes that can stabilize the easy-glide pyramidal dislocations (II or I, or both) throughout the material, delaying the undesirable transitions found here and in earlier work. However, the results here suggest that pyramidal I dislocations are less stable (i.e. have a smaller energy barrier into the undesirable transition) as compared to pyramidal II dislocations. Thus, stabilizing pyramidal II slip is perhaps the most attractive possibility, given the present level of understanding of Mg deformation.

Acknowledgements

Z.W. acknowledges the financial support from the Agency for Science, Technology and Research (A*STAR), Singapore. W.A.C. acknowledges support of this work through a European Research Council Advanced Grant, "Predictive Computational Metallurgy", ERC Grant agreement No. 339081 - PreCoMet. Part of the computer time was supported by a grant from the Swiss National Supercomputing Centre (CSCS) under project ID s631.

References

[1] M. H. Yoo, Metallurgical Transactions A - Physical Metallurgy and Materials Science 12 (1981) 409–418.

[2] S. R. Agnew, C. Bettles, M. Barnett, 2 - Deformation mechanisms of magnesium alloys, Woodhead Publishing, 2012, pp. 63–104.

[3] Z. Wu, W. A. Curtin, Nature 526 (2015) 62–67.

[4] B. Devincre, T. Hoc, L. Kubin, Science 320 (2008) 1745–1748.

[5] N. Bertin, C. N. Tomé, I. J. Beyerlein, M. R. Barnett, L. Capolungo, International Journal of Plasticity 62 (2014) 72–92.

[6] J. F. Stohr, J. P. Poirier, Philosophical Magazine 25 (1972) 1313–1329.

[7] T. Obara, H. Yoshinga, S. Morozumi, Acta Metallurgica 21 (1973) 845–853.

[8] J. Geng, M. F. Chisholm, R. K. Mishra, K. S. Kumar, Philosophical Magazine Letters 94 (2014) 377–386.

[9] J. Geng, M. F. Chisholm, R. K. Mishra, K. S. Kumar, Philosophical Magazine In Press (2015).

[10] J. P. Hirth, J. Lothe, Theory of Dislocations, 2 ed., John Wiley & Sons, 1982.

[11] S. Nosé, Molecular Physics: An International Journal at the Interface Between Chemistry and Physics 52 (1984) 255–268.

[12] S. Nosé, Journal of Chemical Physics 81 (1984) 511–519.

[13] W. G. Hoover, Physical Review A 34 (1986) 2499–2500.

[14] S. Melchionna, G. Ciccotti, B. L. Holian, Molecular Physics: An International Journal at the Interface Between Chemistry and Physics 78 (1993) 533–544.

[15] S. Plimpton, Journal of Computational Physics 117 (1995) 1–19.

[16] Z. Wu, M. F. Francis, W. A. Curtin, Modelling and Simulation in Materials Science and Engineering 23 (2015) 015004.

[17] D. Faken, H. Jónsson, Computational Materials Science 2 (1994) 279–286.

[18] G. Henkelman, H. Jónsson, Journal of Chemical Physics 113 (2000) 9978–9985.

[19] G. Henkelman, B. P. Uberuaga, H. Jónsson, Journal of Chemical Physics 113 (2000) 9901–9904.

[20] S. Sandlöbes, M. Friák, J. Neugebauer, D. Raabe, Materials Science and Engineering: A 576 (2013) 61–68.

[21] S. Ando, A. Kodera, K. Fukushima, M. Tsushida, H. Kitahara, Materials Science Forum 783-786 (2014) 341–345.